活断層・古地震研究報告，No. 22, p. 33-52, 2022

Potential for a large earthquake on the Midorikawa fault zone in the vicinity of the 2016 Kumamoto earthquake sequence, central Kyushu, Japan

MARUYAMA Tadashi[1], YOSHIOKA Toshikazu[1, 2], MUKAI Masashi[3] and HORIKAWA Shigeo[3]

[1]AIST, Geological Survey of Japan, Research Institute of Earthquake and Volcano Geology, tadashi-maruyama@aist.go.jp
[2]Oita Bungoono Geopark Promotion Council, 1200 Miemachi-Ichiba, Bungo Ono, Oita, 879-7198, Japan
[3]Suncoh Consultants Co., Ltd., 1-8-9 Kameido, Koto, Tokyo, 136-8522, Japan

Abstract: The 2016 Kumamoto earthquake caused changes in the crustal stress state in central Kyushu that might affect the timing of large earthquakes on nearby faults. One of those faults is the ENE–WSW-striking active Midorikawa fault zone, ~20 km from the causative fault. Despite the importance of the Midorikawa fault zone for assessing seismic hazards in central Kyushu, its recent behavior is poorly known. Its eastern end features a narrow graben-like depression that displaces pyroclastic flow deposits from Aso Volcano (Aso-4) dated at ~88–87 ka with a net north-side-down vertical offset of 8–10 m, suggesting a vertical slip rate of ~0.1 mm/yr. A paleoseismic trench across the southern edge of this depression at Kariya, Yamato Town, exposed a series of steeply dipping normal faults with a probable dextral component that deform late Pleistocene to Holocene strata. Radiocarbon dating, tephrochronological information, and structural features suggest that the latest surface-rupturing paleoseismic event, with a 2.1 m north-side-down vertical offset, occurred in the age range between *c*. 7,670 cal BP and *c*. 1,740 cal BP, and the preceding surface-rupturing event predates the deposition of the Kusasenrigahama pumice from Aso Volcano (*c*. 30 ka). A 4 m offset of the top of the Aso-4 deposit across the trench section, detected by boreholes, may indicates repeated faulting events. Although the extent of the latest rupture event is unclear, the magnitude of its vertical displacement permits the possibility that the entire fault zone, which is comparable in length to the surface rupture of the Kumamoto earthquake, ruptured simultaneously. Assuming a constant rate of strain accumulation, the Midorikawa fault zone has stored crustal strain corresponding to a vertical slip of ~0.8 m near its eastern terminus.

Keywords: Midorikawa fault zone, 2016 Kumamoto earthquake, paleoseismology, trenching investigation, central Kyushu

1. Introduction

The 2016 Kumamoto earthquake sequence, including the M_W 7.0 (M_{JMA} 7.3) mainshock on 16 April, devastated central Kyushu, Japan, resulting in 273 deaths and more than 2,809 injuries (Fire and Disaster Management Agency, 2019). It was caused primarily by slip on the eastern segment of the Futagawa fault zone and its western and eastern extensions, and the northernmost part of the Hinagu fault zone (e.g., Earthquake Research Committee, the Headquarters for Earthquake Research Promotion (hereafter ERC HERP), 2016; Shirahama *et al*., 2016; Kumahara *et al*., 2017; Suzuki *et al*., 2017) (Fig. 1b). Estimates of the Coulomb stress transfer from this event indicate changes in the crustal stress state in central Kyushu that might affect the timing of large earthquakes on nearby faults (Toda, 2016).

The ENE–WSW-trending Midorikawa fault zone, which extends for ~34 km and lies ~20 km south of the Futagawa fault zone, is one of the nearest active faults to the Futagawa fault zone. It is considered to be a primary active fault in central Kyushu that, given its length, could generate a large (magnitude 7.4) earthquake (ERC HERP, 2013c) (Fig. 1b). The static Coulomb stress on the eastern part of the Midorikawa fault zone appears to have increased as a result of the 2016 earthquake (Toda, 2016). However, its recent faulting history is unknown, which has hampered seismic hazard evaluations in central Kyushu subsequent to the Kumamoto earthquake sequence. Here, we present the results of the first paleoseismological investigation of the Midorikawa fault zone, which was performed in late 2015 and early 2016. This report is mainly based on previous reports by the National Institute of Advanced Industrial Science and Technology (2016) and Togo *et al*. (2016), with some additions and revisions.

2. Geology and geomorphology of the Midorikawa fault zone

Kyushu lies on the Eurasian (or Amur) plate west of the Nankai trough, where the Philippine Sea plate subducts northwestward at a convergence rate of ~70 mm/yr

(Loveless and Meade, 2010) (Fig. 1a). Geodetical observations show that central Kyushu is dominated by N–S extension (Sagiya *et al*., 2000). Given the angle between the strike of the fault and the orientation of extension, the Midorikawa fault zone is considered to have undergone mainly north-side-down normal faulting with a dextral component during the late Quaternary (e.g., Chida, 1980; Research Group for Active Faults of Japan (hereafter RGAFJ), 1980, 1991; The Research Group for Active Tectonics in Kyushu (hereafter RGATK), 1989). This fault zone is partially coincident with the Usuki–Yatsuriho Tectonic Line, a major boundary fault in the Kyushu region that divides southwestern Japan into the outer zone in the south and the inner zone in the north (Iki, 1901; Saito *et al*., 2005, 2010). The Midorikawa fault zone occupies a topographic boundary between the northern slope of the Kyushu Mountains to the south and a plateau to the north that is covered by materials erupted from Aso Volcano (Fig. 1b). Historically, no earthquakes of large or moderate size have been reported on this fault zone.

Previous geomorphological interpretations based on aerial photographs show that the Midorikawa fault zone comprises several faults: from east to west these are the Kamano fault, the Gezu fault, the Kiharadani fault, and the Midorikawa fault (RGAFJ, 1980, 1991; RGATK, 1989; ERC HERP, 2013c) (Fig. 1b). The Kamano fault has the strongest geomorphic expression. Chida (1980), RGAFJ (1980, 1991) and RGATK (1989) reported that the Kamano fault displaces the depositional surface (Surface 1 in Figs. 2 and 3) of pyroclastic flow deposits (Aso-4) from a gigantic eruption of Aso Volcano (e.g., Watanabe, 1978; Machida and Arai, 2003), where it forms a distinct graben-like depression with two nearly parallel fault scarps facing each other; here we refer to the northern (i.e., south-facing) scarp as Kamano I and the southern (north-facing) scarp as Kamano II following RGAFJ (1980, 1991) and RGATK (1989) (Fig. 2). The age of the Aso-4 eruption was recently reported to be 88 ka (Nagahashi *et al*., 2007) and ~87 ka (Aoki, 2008; Smith *et al*., 2013). Based on the vertical offset of Surface 1 by 3 m on the Kamano I fault and 6 m on the Kamano II fault and a depositional age of 70–80 ka for the Aso-4 pyroclastic flow, RGAFJ (1991) estimated long-term vertical slip rates of 0.04 mm/yr for the Kamano I fault and 0.09 mm/yr for the Kamano II fault. The difference between these slip rates corresponds to a net north-side-down vertical slip rate across the Kamano fault zone of 0.05 mm/yr. However, high-resolution digital elevation data from a recent Light Detection And Ranging (LiDAR) survey show that the vertical offsets of surface 1 on the Kamano fault are clearly larger than those reported previously, and the net vertical offset is 8–10 m (Fig. 3). Combining this offset and the revised age of the Aso-4 deposits yields an estimated net vertical slip component of ~0.1 mm/yr on the Kamano fault.

The Gezu, Kiharadani, and Midorikawa faults are marked by prominent topographic lineaments, but there are no topographic features that indicate recent faulting activity (Chida, 1980; RGAFJ, 1980, 1991; RGATK, 1989; Nakata and Imaizumi, 2002). On the Gezu fault, which runs parallel to the Kamano fault a few hundred meters to the south, no fault scarps displace Surface 1, indicating that it has likely been inactive since ~88–87 ka (Fig. 3). The Kiharadani and Midorikawa faults are not amenable to geomorphic analysis because they do not cross any clear geomorphic surfaces of late Pleistocene age. We undertook a paleoseismological investigation including trenching and drilling on the central part of the Kamano II fault, across a distinct north-facing scarp 2 m high (Fig. 4).

3. Paleoseismic trenching

3.1. Description

We excavated a trench 17 m long, 4 m wide, and 4 m deep across the topographic scarp of the Kamano II fault at Kariya, Yamato Town, Kumamoto Prefecture (Figs. 2 and 4). The trench walls were cleaned and gridded at 0.5 m (horizontal) × 1 m (vertical) spacing and logged at a scale of 1:20 (Figs. 5–7).

The trench walls exposed eolian sediments and soils, including weathered tephric loess deposits, a tephra fall layer, organic-rich paleosols, and fissure fills. We divided them into five stratigraphic units on the basis of sedimentary facies (Units 1 to 5 from top to bottom) plus Unit α, representing fissure fill. Units 1 and 2 were further divided into subunits on the basis of differences in color and grain size (Figs. 5 and 6). Features of each unit and subunit are summarized in Table 1.

Among these units, which are predominantly gray to black soils and tephric loess deposits, Unit 3 stands out as an orange to dark orange layer 20–30 cm thick composed mainly of well-sorted pumice clasts 2 to 6 mm in diameter. We identified Unit 3 as the Kusasenrigahama pumice fall layer (Kpfa), erupted *c*. 30 ka from Aso Volcano (Watanabe *et al*., 1982; Miyabuchi *et al*., 2003; Miyabuchi, 2009), on the basis of tephra analyses performed for the overlying unit (Unit 2) described below and its consistency with the mapped thickness distribution of Kpfa (Fig. 1b). The trench walls clearly exposed a series of four north-side-down faults at the base of the topographic scarp (Figs. 4–7), which we refer to as Faults *F1* to *F4* from north to south. The east and west walls of the trench were quite similar.

3.2. Deformation of strata

Our examination of the trench showed that Faults *F1* to *F4* each consist of multiple strands with various dips and dip directions, but all have near-vertical dips and display offsets down to the north (Figs. 5 and 6). Each fault is accompanied by fissures of various sizes filled by material of Unit α. Signs of dextral slip on the floor of the trench include shear fabric and asymmetric spindle-shaped depressions filled by Unit α (Fig. 8). These structural features define the Kamano II fault as a steeply dipping extensional normal fault zone with a dextral slip component.

Faults *F1* to *F4* and their associated fissures affect units up to and including Unit 1c, but their apparent vertical offsets do not affect Unit 1b (Figs. 5 and 6). Fault *F1*, a set of several steeply dipping faults, displaces Units 5 to 1c but not Unit 1b (Fig. 5). Its offsets of the bases of Units 4 through 2a are nearly uniform (0.6 to 0.8 m) (Figs. 5 and 6). Fault *F2* consists of two steeply dipping faults that bound a fissure that ends at Unit 1b (Fig. 5). Fault *F3* appears on the west wall as a north-dipping fault and a south-dipping subsidiary fault that define a small horst-like mound (Fig. 5). The deformation of Fault *F3* varies from a distinct displacement below Unit 2b to a gentle warping in Units 2b and 2a, but its offsets are similar (0.5 to 0.8 m) at the tops of Units 4 to 2a. Fault *F4*, like Fault *F3*, varies from a distinct displacement in Units 5 through 3 to a gentle warping in Unit 2a (Figs. 5 and 6). It offsets the base of Units 3 and 2b by 0.8 m and the base of Unit 2a by less than 0.3 m.

3.3. Age control

We performed AMS radiocarbon dating and tephra analyses to constrain the age of the stratigraphic units and the timing of paleoseismic events. Lacking particles of wood or charcoal, we used bulk samples of organic sediment from some units, including Unit α, for radiocarbon analysis (Table 2, Fig. 5). These showed consistency between stratigraphic positions and ages.

We took tephra samples at 10 cm intervals from Units 2b and 2a in grids W6.7 (TLW1) and W2.7 (TLW2) of the west wall (Table 3, Fig. 5). Mineral counts, characterizations of volcanic glass surfaces, and refractive index determinations were conducted following the procedure of Furusawa (1995). The results show that the widespread Aira-Tn (AT) tephra from Aira Caldera (*c*. 30 ka; Smith *et al*., 2013; Fig. 1a) is concentrated in the lower half of Unit 2a, suggesting that this unit was deposited at or near the time of the AT eruption. The lower half of Unit 2a lies 0.5 to 1 m above the top of the thick tephra in Unit 3 (Fig. 5) consistent with the occurrence of the Kpfa tephra 0.5 to 1 m below AT elsewhere around Aso Volcano (Miyabuchi *et al*., 2003). This evidence strongly suggests that Unit 3 is the Kpfa tephra. The tephrochronological evidence from Units 2a and 3 is inconsistent with the younger radiocarbon date obtained for the underlying Unit 4 (sample CW14 in Table 2), which may reflect the presence of young carbon. We therefore relied on tephrochronology to constrain the timing of the paleoearthquakes discussed below.

3.4. Paleoseismic events

Details of the trench exposures allowed us to identify a paleoseismic event horizon, which represents the ground surface at the time of a paleoearthquake. The fissures associated with Faults *F1* to *F4* are filled by Unit α, composed of fragments of Units 2a, 1d, and 1c. Furthermore, Units 1d and 1c are nearly absent between Faults *F1* and *F4*, whereas they are present to the north of Fault *F1* and to the south of Fault *F4* (Figs. 5 and 6). We interpret these findings as the result of the formation of fissures during surface faulting that occurred after the deposition of Unit 1c. Near-surface materials of Units 2a, 1d, and 1c filled the fissures immediately, followed by the collapse and erosion of the fault scarp (Fig. 9a). This interpretation is supported by the radiocarbon ages of Unit α (samples CW8, CW9, CW11), which are consistent with those from Units 1d (samples CW3, CW7, CW15) and 1c (sample CW5) (Table 2). Indeed, Unit 1b covers the tops of the fissures and is not present within them (Figs. 5, 6, and 9a).

The trench revealed no clear evidence for any preceding scarp-forming events, such as angular unconformities, colluvial wedges, abrupt changes in stratal deformation, and liquefaction features (Figs. 4 and 5). The possible exceptions are the variation of apparent vertical offsets across Fault *F4*, mentioned above, and the upward termination of Faults *F3* and *F4* within Unit 2b. These would be consistent with an event (hereafter the possible event) with a small north-side-down vertical offset that occurred after or during the deposition of Unit 2b and before the deposition of Unit 2a (Fig 9b). However, we consider such an event unlikely for several reasons (Fig. 9a). First, Unit 2 is a weathered volcanic ash (weathered tephric loess deposit) that developed on an unstable north-facing slope, accounting for its variable thickness as shown in Fig. 10, and it cannot be considered a reliable recorder. Second, the vertical offset of the base of Unit 2a in the east wall, a broad deformation above the upper tip of Fault *F4*, appears not to differ from the offsets of the bases of underlying Units 2b and 3 (Fig. 6). Third, between grids E7 and E8, Unit α fills the fissure formed by the latest event but does not cut Fault *F4*, and instead appears to fill a branch of Fault *F4*. Fourth, although

numerous distinct fissures are connected to the latest event horizon, none are evident at other stratigraphic levels on Faults *F3* and *F4*. Fifth, no colluvium that would be expected to be shed from a fault scarp is present in Unit 2b on the downthrown side of Faults *F3* and *F4*. Sixth, the difference in vertical offsets between Units 2b and 2a may be an artifact of strike-slip faulting during the latest event, as observed on the trench floor. Seventh, if the strike-slip component of faults exposed in the trench is substantial, given the fact that most strike-slip fault strands have been reported to die out before reaching the ground surface at the time of the earthquake, it is not appropriate to consider the disappearance of Faults *F3* and *F4* within Unit 2b as evidence of an independent event without other paleoseismic indicators like scarp colluvium or fissures (McCalpin *et al*., 2009).

Our preferred interpretation of this evidence is that the latest event at the trench site postdates the deposition of Unit 1c and predates the deposition of Unit 1b, and the preceding event predates the deposition of the oldest unit (Unit 5) in the trench. Radiocarbon dating of samples from Units 1c (CW5) and 1b (CW12) constrains the timing of the latest event to between *c*. 7,670 cal BP and *c*. 1,740 cal BP (Table 1, Fig. 9a). The inferred age of the tephra in Unit 3 constrains the preceding event to be older than *c*. 30 ka (Table 2). If the possible event postdated the deposition of Unit 2b and predated the deposition of Unit 2a, its timing would be *c*. 30 ka based on the ages of Unit 3 and the lower part of Unit 2a. The vertical offset during the latest event is estimated to be 2.1 m based on the offset of the base of Unit 3 (Fig. 10). If the possible event did occur, this vertical offset corresponds to the cumulative displacement of the two events. The steep dip of the fault surfaces and the shear fabric exposed on the trench floor suggest that dextral slip also occurred during the latest event, but its amount is indeterminate.

4. Drilling survey

We obtained four drill cores, ranging in depth from 9.0 m to 11.0 m, in a section perpendicular to the scarp (Fig. 4a): Cores N-1 and N-2 on the downthrown side and Cores-S1 and S-2 on the upthrown side. All of the cores contain an orange pumice layer that correlates with Unit 3 in the trench, and all of them bottom out in pyroclastic flow deposits (Fig. 10). The pyroclastic flow deposits consist of dacitic rocks and volcanic ash. The rocks include pumice, volcanic glass particles, and crystal fragments. The uppermost part of the deposits is an orange nonwelded tuff breccia. This material is similar to Aso-4 pyroclastic flow deposits elsewhere (e.g., Saito *et al*., 2005). The top of these deposits deepens to the north by 4 m between Cores S-2 and N-2, near the downward extension of the normal faults exposed in the trench. This is consistent with repeated faulting events since the late Pleistocene, although a non-tectonic origin of the 4 m drop, such as erosion or mass movements, is not precluded.

5. Discussion and implications

Our study suggests that the Kamano II fault, an eastern section of the Midorikawa fault zone, ruptured once during the Holocene with a vertical offset of 2.1 m. It is likely that its counterpart across the linear depression, the Kamano I fault, ruptured simultaneously. If the vertical component of slip rate on the Kamano II fault is twice as great as that of the Kamano I fault (as reported by previous studies) or greater (as shown in Fig. 3), the net vertical offset of the entire Kamano fault associated with this event is≥1.2 (~2.1) m. This net vertical offset, estimated near the eastern terminus of the Midorikawa fault zone, is comparable to the measured surface offsets along the ~34 km of surface ruptures associated with the 2016 Kumamoto earthquake, although those displayed primarily lateral offsets (e.g., Shirahama *et al*., 2016; Kumahara *et al*., 2017) (Fig. 1b). The similar amounts of slip during the Holocene event on the Kamano fault and the 2016 Kumamoto earthquake sequence might suggest that the entire length of the Midorikawa fault zone ruptured simultaneously during its latest event, although distinct geomorphic evidence of this event is lacking in the central and western parts of the fault zone. The lack of such evidence may be attributed to high erosion and deposition rates in this mountainous region combined with the low slip rate and long recurrence interval of surface-rupturing earthquakes on the fault zone. If the vertical offset of 2.1 m was the cumulative displacement of two events including the possible event, the rupture extent might have been much smaller for each individual event.

The recurrence of a large earthquake equivalent to the latest event is probably not imminent, considering the short elapsed time since the latest event (*c*. 1,810 yr to *c*. 7,740 yr) compared to the interval since the preceding event (at least *c*. 22,330 yr to *c*. 28,260 yr), and assuming that this fault displays characteristic and periodic seismic behavior (e.g., Shimazaki and Nakata, 1980; Schwartz and Coppersmith, 1984). Such an evaluation would remain largely unchanged even in the existence of the possible event. However, recent paleoseismological studies have shown that surface-rupturing earthquakes on major active faults (or segments) occur more irregularly or in clusters, some of which are probably triggered by ruptures on nearby faults (e.g., Litchfield *et al*., 2010; Rockwell,

2010). If we extend the net vertical slip rate of ~0.1 mm/yr over the elapsed time since the latest event on the Kamano II fault, then the Midorikawa fault zone has stored crustal strain corresponding to a vertical slip of up to 0.8 m near its eastern terminus. Such an event could cause widespread damage in central Kyushu from landslides and slope failures like those that occurred in elevated areas during the 2016 Kumamoto earthquake sequence (e.g., Dai *et al*., 2017; Tajima *et al*., 2017). Further paleoseismic studies on the Kamano and related faults are needed to properly unravel the past behavior and evaluate the future activity of the Midorikawa fault zone.

Acknowledgements

This study was conducted as a part of the research project "Active fault research for regional evaluation, Kyushu region" funded by the Ministry of Education, Culture, Sports, Science and Technology (MEXT), Japan, in the 2015 fiscal year. Figs. 2 and 3 were created using the airborne lidar-derived 1-m grid digital elevation model provided by the Geospatial Information Authority of Japan (GSI). We thank Tetsuhiro Togo for his participation in this study and Tatsuji Matsuzaki for assistance in the field. We thank the landowner of the Kariya site, who provided access to the land for our trenching and drilling work. We are grateful to Yasuo Awata, Yildirim Dilek, Nicola Litchfield, Yukari Miyashita, and Yuichi Sugiyama for constructive comments on early versions of the manuscript. The manuscript was improved by comments from two anonymous reviewers.

References

Aoki, K. (2008) Revised age and distribution of ca. 87 ka Aso-4 tephra based on new evidence from the northwest Pacific Ocean. *Quaternary International*, **178**, 100–118.

Bronk Ramsey, C. (2001) Development of the radiocarbon program. *Radiocarbon*, **43**, 355–363.

Bronk Ramsey, C. (2009) Bayesian analysis of radiocarbon dates. *Radiocarbon*, **51**, 337–360.

Chida, N. (1980) Recent crustal movement in central Kyushu. In Executive committee for commemorative project on the retirement of Prof. Kasuke Nishimura ed., *Memorial volume on celebration for the retirement of Prof. Kasuke Nishimura*. Kokon-Shoin, Tokyo, 89–93 (in Japanese).

Dai, Z., Wang, F., Song, K. and Iio, A. (2017) A first look at a landslide triggered by the 2016 Kumamoto earthquake near the Aso Volcanological Laboratory. *Quarterly Journal of Engineering Geology and Hydrogeology*, **50**, 111–116.

Earthquake Research Committee, the Headquarters for Earthquake Research Promotion (2013a) *Long-term evaluation of active faults in the Kyushu region* (1st version). 81 p (in Japanese), https://www.jishin.go.jp/main/chousa/13feb_chi_kyushu/k_honbun.pdf (Accessed: 2022-07-29).

Earthquake Research Committee, the Headquarters for Earthquake Research Promotion (2013b) *Long-term evaluation of the Futagawa and Hinagu fault zones* (partial revision). 66 p (in Japanese), https://www.jishin.go.jp/main/chousa/katsudansou_pdf/93_futagawa_hinagu_2.pdf (Accessed: 2022-07-29).

Earthquake Research Committee, the Headquarters for Earthquake Research Promotion (2013c) *Long-term evaluation of the Midorikawa fault zone*. 12 p (in Japanese), http://jishin.go.jp/main/chousa/13feb_chi_kyushu/k_12.pdf (Accessed: 2022-07-29).

Earthquake Research Committee, the Headquarters for Earthquake Research Promotion (2016) *Evaluation of the 2016 Kumamoto Earthquakes* (in Japanese)], https://www.static.jishin.go.jp/resource/monthly/2016/2016_kumamoto_3.pdf (Accessed: 2022-07-29).

Fire and Disaster Management Agency (2019) Earthquakes with hypocenters in the Kumamoto district, Kumamoto Prefecture (121st report) (in Japanese), https://www.fdma.go.jp/disaster/info/items/kumamoto.pdf (Accessed: 2022-07-29).

Furusawa, A. (1995) Identification of tephra based on statistical analysis of refractive index and morphological classification of volcanic glass shards. *The Journal of the Geological Society of Japan*, **101**, 123–133 (in Japanese with English abstract).

Iki, T. (1901) Geological structure of central Kyushu. *The Journal of the Geological Society of Japan*, **8**, 80–93 (in Japanese).

Japan Meteorological Agency (2018) *Lists of hypocenters* (in Japanese), http://www.data.jma.go.jp/svd/eqev/data/daily_map/index.html (Accessed: 2022-07-29).

Kishimoto, K. (1999) Combined Bathymetric and Topographic Mesh Data: Japan250m.grd. GSJ Open-file Report No. 353, Geological Survey of Japan, 1 CD-ROM.

Kumahara, Y., Okada, S., Kagohara, K., Kaneda, H., Goto. H. and Tsutsumi, H. (2017) 1:25,000 Active Fault Map, Futagawa-Hinagu Fault Zone and its vicinity, "Kumamoto" (revised edition). Geospatial Information Authority of Japan.

Litchfield, N., van Dissen, R., Hemphill-Haley, M., Townsend, D. and Heron, D. (2010) Post c. 300 year rupture of the Ohariu Fault in Ohariu Valley, New Zealand. *New Zealand Journal of Geology and Geophysics*, **53**, 43–56.

Loveless, J. P. and Meade, B. J. (2010) Geodetic imaging of plate motions, slip rates, and partitioning of deformation in Japan. *Journal of Geophysical Research*, **115**, B02410.

Machida, H. and Arai, F. (2003) *Atlas of Tephra in and around Japan* (revised edition). University of Tokyo Press, Tokyo, 336 p (in Japanese).

McCalpin, J. P., Rockwell, T. K. and Weldon II, R. J. (2009) Chapter 6 Paleoseismology of Strike‐Slip Tectonic Environments. *In* McCalpin, J. P. ed., *Paleoseismology 2nd ed*., International Geophysics, Elsevier, **95**, 421–496.

Ministry of Education, Culture, Sports, Science and Technology and Kyushu University (2017) *A comprehensive active fault research following the 2016 Kumamoto earthquake*. 2016 Fiscal year report, 270 p (in Japanese), https://www.jishin.go.jp/main/chousakenkyuu/kumamoto_sogochousa/h28/h28kumamoto_sogochousa_all.pdf (Accessed: 2022-07-29).

Miyabuchi, Y. (2009) A 90,000-year tephrostratigraphic framework of Aso Volcano, Japan. *Sedimentary Geology*, **220**, 169–189.

Miyabuchi, Y., Hoshizumi, H., Takada, H., Watanabe, K. and Xu, S., (2003) Pumice-fall deposits from Aso volcano during the past 90,000 years, southwestern Japan. *Bulletin of the Volcanological Society of Japan*, **48**, 195–214 (in Japanese with English abstract).

Nagahashi, Y., Sato, T., Takeshita, Y., Tawara, T. and Kumon, F. (2007) Stratigraphy and chronology of widespread tephra beds intercalated in the TKN-2004 core sediment obtained from the Takano Formation, Central Japan. *The Quaternary Research*, **46**, 305–325 (in Japanese with English abstract).

Nakata, T. and Imaizumi, T. (2002) *Digital Active Fault Map of Japan*. University of Tokyo Press, Tokyo, 60 p (in Japanese).

National Institute of Advanced Industrial Science and Technology (2016) 4. The Midorikawa fault zone. Active fault research for regional evaluation–Kyushu region–FY 2015 Results Report (in Japanese), 40 p, https://www.jishin.go.jp/main/chousakenkyuu/chiiki_chousa/h27_midorikawa.pdf (Accessed: 2022-07-29).

Reimer, P. J., Austin, W. E. N., Bard, E., Bayliss, A., Blackwell, P. G., Bronk Ramsey, C., Butzin, M., Cheng, H., Edwards, R. L., Friedrich, M., Grootes, P. M., Guilderson, T. P., Hajdas, I., Heaton, T. J., Hogg, A. G., Hughen, K. A., Kromer, B., Manning, S. W., Muscheler, R., Palmer, J. G., Pearson, C., van der Plicht, J., Reimer, R. W., Richards, D. A., Scott, E. M., Southon, J. R., Turney, C. S. M., Wacker, L., Adolphi, F., Büntgen, U., Capano, M., Fahrni, S. M., Fogtmann-Schulz, A., Friedrich, R., Köhler, P., Kudsk, S., Miyake, F., Olsen, J., Reinig, F., Sakamoto, M., Sookdeo, A. and Talamo, S. (2020) The IntCal20 northern hemisphere radiocarbon age calibration curve (0–55 cal kBP). *Radiocarbon*, **62**, 725–757.

Research Group for Active Faults of Japan (1980) *Active Faults in Japan: Sheet Maps and Inventories*. University of Tokyo Press, Tokyo, 363 p (in Japanese with English summary 2 p).

Research Group for Active Faults of Japan (1991) *Active Faults in Japan: Sheet Maps and Inventories* (revised edition). University of Tokyo Press, Tokyo, 437 p (in Japanese with English summary 3 p).

Rockwell, T. (2010) The non-regularity of earthquake recurrence in California: Lessons from long paleoseismic records from the San Andreas and San Jacinto faults in southern California, and the North Anatolian fault in Turkey. *International Conferences on Recent Advances in Geotechnical Earthquake Engineering and Soil Dynamics*. **5**. http://scholarsmine.mst.edu/icrageesd/05icrageesd/session13/5 (Accessed: 2022-07-29).

Sagiya, T., Miyazaki, S. and Tada, T. (2000) Continuous GPS array and present-day crustal deformation of Japan. Pure and Applied Geophysics, **157**, 2303–2322.

Saito, M., Miyazaki, K., Toshimitsu, S. and Hoshizumi, H. (2005) *Geology of the Tomochi district. Quadrangle Series, 1:50 000*, Geological Survey of Japan, AIST, 218 p (in Japanese with English abstract 8 p).

Saito, M., Takarada, S., Toshimitsu, S., Mizuno, K., Hoshizumi, H., Hamasaki, S., Sakaguchi, K. Ohno, T. and Murata, Y. (2010) *Geological Map of Japan 1:200 000, Yatsushiro and a part of Nomo Zaki*. Geological Survey of Japan, AIST, NI-52-12, 18.

Schwartz, D. P. and Coppersmith K. J. (1984) Fault behavior and characteristic earthquakes: Examples from the Wasatch and San Andreas fault zones. *Journal of Geophysical Research*, **89**, 5681–5698.

Shimazaki, K. and Nakata, T. (1980) Time-predictable recurrence model for large earthquakes. *Geophysical Research Letters*, **7**, 279–282.

Shirahama, Y., Yoshimi, M., Awata, Y., Maruyama, T., Azuma, T., Miyashita, Y., Mori, H., Imanishi, K., Takeda, N., Ochi, T., Otsubo, M., Asahina, D. and Miyakawa, A. (2016) Characteristics of the surface ruptures associated with the 2016 Kumamoto earthquake sequence, central Kyushu, western Japan. *Earth Planets and Space*, **68**:191.

Smith, V. C., Staff, R. A., Blockley, S. P. E., Bronk Ramsey, C., Nakagawa, T., Mark, D. F., Takemura, K., Danhara, T. and Suigetsu 2006 Project Members (2013) Identification and correlation of visible tephras in the Lake Suigetsu SG06 sedimentary archive, Japan: chronostratigraphic markers for synchronising of east Asian/west Pacific palaeoclimatic records across the last 150 ka., *Quaternary Science Reviews*, **67**, 121–137.

Suzuki, Y., Ishimura, D., Kumaki, Y., Kumahara, Y., Chida, N., Nakata, T and Nakano, T. (2017) 1:25,000 Active Fault Map, Futagawa-Hinagu Fault Zone and its vicinity, "Aso" (revised edition). Geospatial Information Authority of Japan.

Tajima, Y., Hasenaka, T. and Torii, M. (2017) Effects of the 2016 Kumamoto earthquakes on the Aso volcanic edifice. *Earth, Planets and Space,* **69**:63.

The Research Group for Active Tectonics in Kyushu (1989) *Active Tectonics in Kyushu*. University of Tokyo Press, Tokyo, 553 p (in Japanese with English summary 4 p).

Toda, S. (2016) Static stress change and off-fault aftershocks associated with the 2016 Kumamoto earthquake. *Report of the Coordinating Committee for Earthquake Prediction (CCEP)*, 96, 668–670 (in Japanese), http://cais.gsi.go.jp/YOCHIREN/report/kaihou96/12_25.pdf (Accessed: 2022-07-29).

Togo, T., Yoshioka, T., Mukai, O. and Horikawa, S. (2016) Trench excavation survey of the Midorikawa fault zone, Kumamoto Prefecture, Japan. *Programme and Abstracts, JSAF 206 Fall Meeting*, Japan Society for Active Fault Studies, P-19 (in Japanese with English title).

Watanabe, K. (1978) Studies on the Aso pyroclastic flow deposits in the region to the west of Aso caldera, southwest Japan, I: Geology. *Memoirs of the Faculty of Education Kumamoto University*, 27, 97–120.

Watanabe, K., Ono, K. and Hiratsuka, S. (1982) Pumice deposits from Kusasenrigahama Volcano, Aso caldera. *Bulletin of the Volcanological Society of Japan*, **27**, 337–338 (in Japanese).

（受付:2022 年 8 月 30 日, 受理:2022 年 11 月 17 日）

【追加】

2016 年熊本地震の起震断層に近接する緑川断層帯における大地震の可能性

丸山　正・吉岡　敏和・向井　理史・堀川　滋雄

緑川断層帯は，九州中部の地震災害を評価する上で重要な活断層であるにもかかわらず，最近の活動は不明である．断層帯東端部では，Aso-4 火砕流堆積物からなる地形面に発達する地溝状の凹地を横切る上下方向の平均変位速度は約 0.1 mm/yr と見積もられる．山都町仮屋地区で実施したトレンチ調査の結果，後期更新世から完新世の地層を変形させる複数の正断層が認められた．約 2.1 m 北側落下の変位を伴う最新イベントが約 7,670 cal BP から約 1,740 cal BP の間に発生し，先行するイベントが約 30 ka より前に発生したと考えることが妥当と解釈した．群列ボーリングで検出された Aso-4 上端の約 4 m の北側下りの高低差は，断層活動の繰り返しを示す可能性がある．最新活動時には，熊本地震の地震断層の規模に匹敵する断層帯全体が破断した可能性がある．断層周辺の歪の蓄積速度が一定と仮定すると，緑川断層帯東端部では最大約 0.8 m の上下変位を伴う活動が生じる可能性がある．

Table 1. Stratigraphic units exposed in the trench at the Kariya site.

Stratigraphic unit	Environment	Color	Description
0	Artificial fill	Black, dark brown and light brown	Mainly organic sandy silt including abundant tephric silt blocks. Contains roots, wood and bamboo fragments, and artificial materials.
1a	Soil	Black	Highly organic silty sand. Mainly very fine to fine grained tephra. Unit was removed in most of the trench due to early construction work.
1b	Soil	Black	Highly organic sandy silt. Mainly very fine to fine grained tephric loess. Exposed only north of grids W8 and E10. Thickness 30–40 cm. Overlies Faults *F1* and *F2* and related fissures.
1c	Soil	Blackish brown	Clayey silt containing abundant very fine to fine grained tephra. Exposed only north of grids W11 and E12 and at the south end of the trench. Thickness 20–40 cm; gradually thickens to the north. Contains minor orange glassy tephra in the middle to lower part. Boundary with underlying Unit 1d is unclear and usually gradual.
1d	Soil	Black	Highly organic clayey silt. Mainly exposed north of grids W11 and E10; partly exposed south of grids W1 and E2. Thickness 20–40 cm; gradually thickens to the north. Boundary with underlying Unit 2a is generally indistinct and highly undulate.
2a	Weathered tephric loess	Light yellowish brown to yellowish brown	Mainly silt and abundant fine to very fine sand. Exposed throughout the trench. Thickness varies widely owing to undulating boundary with underlying Unit 2b. Thickness is 70–90 cm south of grids W6 and E7 and 80–110 cm north of grids W6 and E7. Numerous subvertical cracks filled by clayey silt–sand present in upper part. Contains cryptotephra correlated with *c*. 30 ka Aira-Tn (AT) tephra.
2b	Weathered tephric loess	Greenish dark yellow brown	Sandy silt to sandy clay, containing fine to medium sand and sporadic coarse sand and granules. Boundary with underlying Unit 3 is indistinct and strongly undulating. Thickness varies from 50–70 cm south of grids W6 and E7 to 70–80 cm north of grids W6 and E7.
3	Pumice fall	Orange to dark orange	Mainly well-sorted pumice containing 2–6-mm-diameter clasts (*c*. 30 ka Kusasenrigahama pumice). Generally weathered to clay. Thickness 20–30 cm; slightly thicker on the west wall.
4	Paleosol	Greenish dark yellow gray	Organic clay. Mainly clay; organics in upper part. Thickness 20–30 cm. Boundary with underlying Unit 5 is gradual.
5	Weathered tephric loess	Light grayish yellow	Mainly homogeneous massive silty clay. Thickness ≥80 cm. Exposed south of grids W10 and E10.
α	Fissure fill	Black to dark brown	Organic clay with numerous fragments of Units 2a, 1d, and 1c.

Table 2. AMS radiocarbon dating results for samples from the west wall of the trench at the Kariya site[*].

Sample number	Stratigraphic unit	Lab. Number	$\delta^{13}C$ (‰)	Conventional ^{14}C age (^{14}C BP) (±1σ)	Calibrated age range (cal BP) (95.4% probability)	
CW4	1b	Beta-431250	–15.4	1,130 ± 30	1,080–950 1,120–1,090 1,180–1,160	(88.9%) (3.5%) (3.0%)
CW12	1b	Beta-431256	–17.1	1,930 ± 30	1,930–1,740	(95.4%)
CW5	1c	Beta-431251	–20.4	6,720 ± 30	7,540–7,510 7,670–7,560	(17.3%) (78.2%)
CW3	1d	Beta-431249	–20.4	8,670 ± 30	9,690–9,540	(95.4%)
CW15	1d	Beta-431258	–20.9	9,010 ± 40	9,990–9,960 10,030–10,010 10,070–10,040 10,250–10,120	(4.6%) (0.7%) (2.5%) (87.7%)
CW7	1d	Beta-431252	–20.9	9,280 ± 30	10,320–10,300 10,580–10,330	(2.6%) (92.8%)
CW14	4	Beta-431257	–19.6	23,370 ± 90	27,760–27,350	(95.4%)
CW9	α	Beta-431254	–21.7	7,710 ± 30	8,550–8,410 8,590–8,570	(93.6%) (1.9%)
CW8	α	Beta-431253	–21.1	8,200 ± 30	9,280–9,020	(95.4%)
CW11	α	Beta-431255	–21.2	8,250 ± 30	9,050–9,030 9,110–9,090 9,330–9,120 9,410–9,350	(2.1%) (1.8%) (82.6%) (9.0%)

[*] Analyses by Beta Analytic Inc., Miami. All samples consisted of organic sediment and were pretreated with an acid wash. Conventional age calculations assume Libby half-life of 5,568 yr. Calibrations were done with OxCal v. 4.4 (Bronk Ramsey, 2001, 2009) and the IntCal20 atmospheric curve (Reimer *et al*. 2020). All ages are rounded to the nearest decade.

Table 3. Results of tephra analyses for two columnar samples from the west wall of the trench at the Kariya site.

Sample number	Volcanic glass types (per 3,000 grains)*			Heavy minerals (per 3,000 grains)†			β quartz (per 3,000 grains)‡	Reflective index of volcanic glass (*n*)	Identified tephra
	Bw	Pm	O	Opx	Gho	Cum			
LW1-17	243	2	15	274	21	0	0.1		
LW1-16[a]	196	4	14	183	23	0	0.0		
LW1-15	221	17	19	205	26	0	0.0		
LW1-14	284	13	43	220	30	0	0.1	1.497-1.504 (mode 1.497-1.500)	Aira–Tn
LW1-13	733	11	50	167	42	0	0.3	1.497-1.501	Aira–Tn
LW1-12	803	21	94	137	46	0	0.2	1.497-1.503 (mode 1.497-1.501)	Aira–Tn
LW1-11	542	20	59	216	53	0	0.3	1.497-1.501	Aira–Tn
LW1-10	916	24	115	122	57	0	0.0	1.497-1.501	Aira–Tn
LW1-9	1031	28	55	146	40	0	0.1	1.497-1.501	Aira–Tn
LW1-8	360	39	47	243	22	0	0.0		
LW1-7	59	22	41	364	6	0	0.0		
LW1-6	9	22	40	382	3	0	0.1		
LW1-5[b]	5	52	64	308	0	0	0.0		
LW1-4	1	50	22	225	2	0	0.0		
LW1-3	6	34	36	306	3	0	0.0		
LW1-2	18	115	28	202	1	0	0.0		
LW1-1	7	193	15	291	0	0	0.0		
LW2-11c	254	2	14	301	19	0	0		
LW2-11b	253	6	21	361	28	0	0		
LW2-11a	305	3	13	366	41	0	0.1	1.497-1.501	Aira–Tn
LW2-10a	491	9	21	186	28	0	0.1	1.497-1.501	Aira–Tn
LW2-9a	610	15	32	153	59	0	0.1	1.497-1.501	Aira–Tn
LW2-8	682	12	41	151	48	0	0.3	1.497-1.501	Aira–Tn
LW2-7	621	12	50	190	70	0	0.3	1.497-1.501	Aira–Tn
LW2-6	797	21	125	247	22	0	0.1	1.497-1.501	Aira–Tn
LW2-5	230	30	40	351	10	0	0		
LW2-4	9	9	53	468	4	0	0		
LW2-3	0	19	57	459	3	0	0		
LW2-2	5	75	8	493	1	0	0		
LW2-1	7	82	6	382	1	0	0		

* Bw, bubble wall shape; Pm, pumice shape; O, other type.

† Opx, orthopyroxene; Gho, green hornblende; Cum, cummingtonite.

‡ Converted from counts per approximately 20,000 grains.

[a] Contains minor olivine.

[b] Contains abundant pale reddish-brown poorly vesiculated volcanic glass.

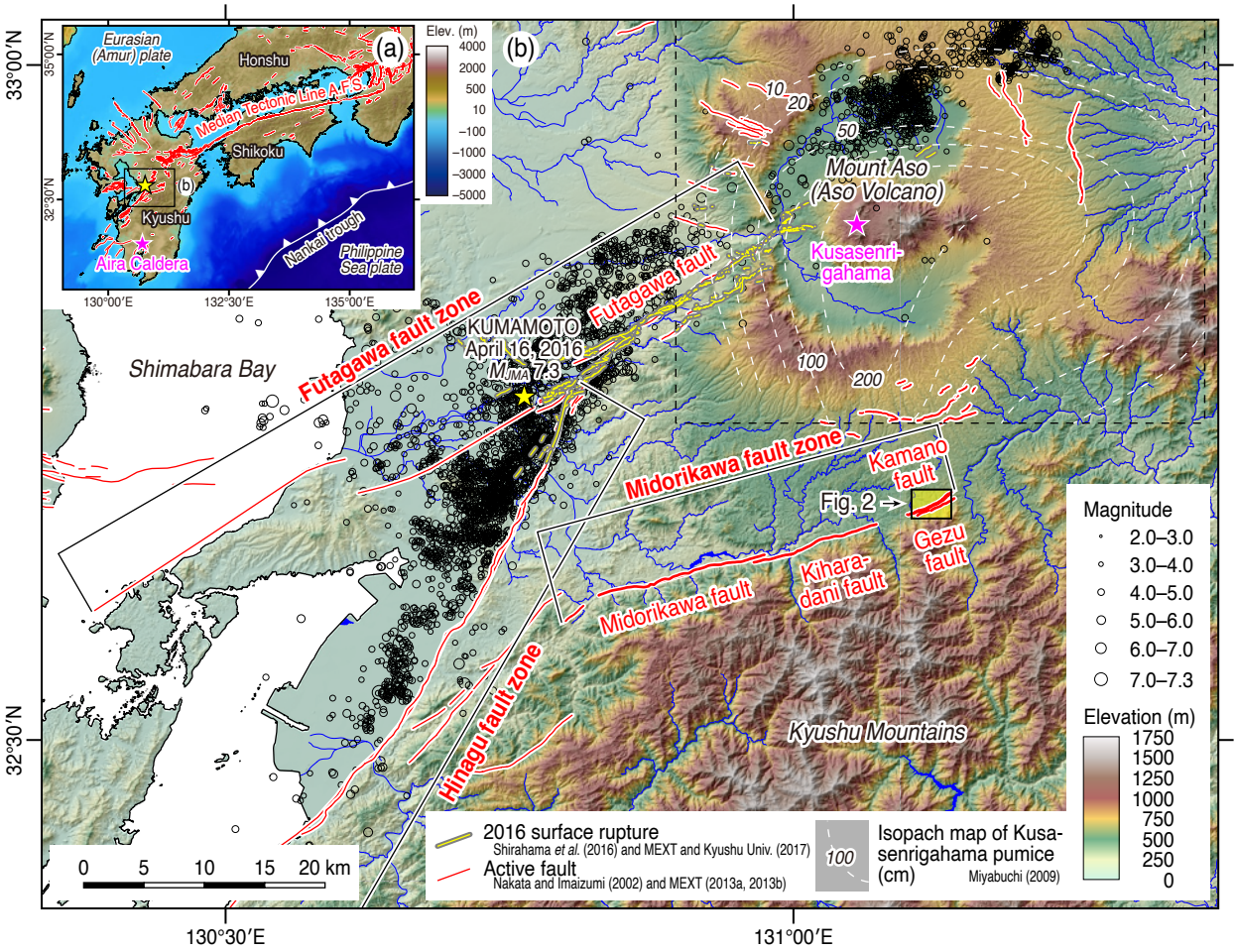

Fig. 1. (a) Location map showing the tectonic setting and active faults in southwestern Japan. A.F.S.: active fault system. Yellow and magenta stars denote the mainshock epicenter of the 2016 Kumamoto earthquake (Japan Meteorological Agency, 2018) and the location of Aira Caldera, respectively. Background topography and bathymetry is after Kishimoto (1999). Active fault traces are from Nakata and Imaizumi (2002) and ERC HERP (2013a). (b) Topographic map showing the locations of the major active faults in central Kyushu and Aso Volcano. Active fault traces are from Nakata and Imaizumi (2002) and ERC HERP (2013b, 2013c). Fault names are after ERC HERP (2013c). A yellow star denotes the mainshock epicenter of the 2016 Kumamoto earthquake (Japan Meteorological Agency, 2018). Surface ruptures associated with the Kumamoto earthquake sequence are simplified from Shirahama *et al*. (2016) and Ministry of Education, Culture, Sports, Science and Technology (MEXT) and Kyushu University (2017). Black circles are epicenters of earthquakes (M≥2.0 with focal depths shallower than 30 km) between 14 and 30 April 2016 (Japan Meteorological Agency, 2018). A magenta star denotes the location of Kusasenrigahama Volcano, source of the Kusasenrigahama pumice (Kpfa). Isopachs of Kpfa in the dashed black rectangle are after Miyabuchi (2009). Topography is from the 10-m mesh digital elevation model issued by Geospatial Information Authority of Japan.

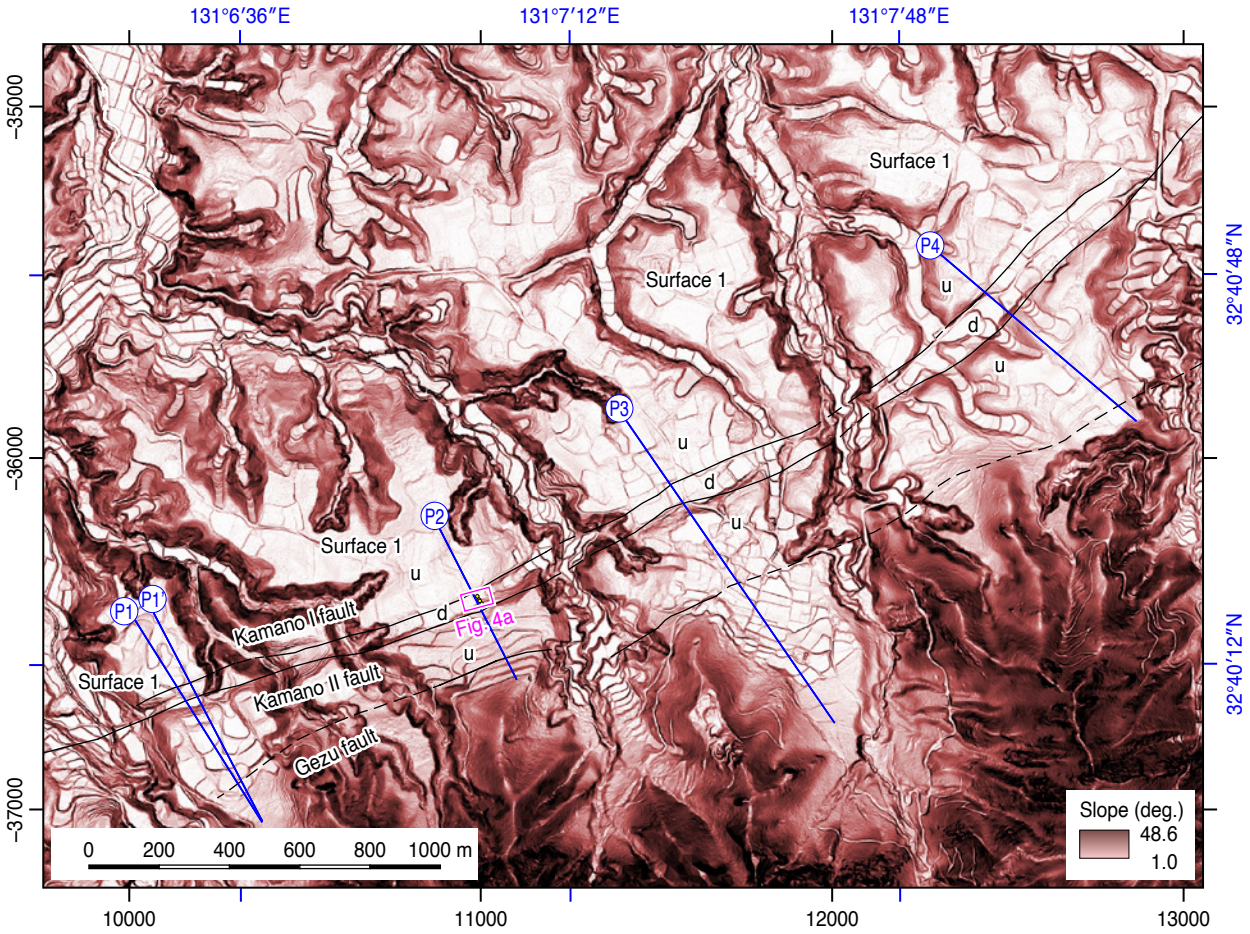

Fig. 2. Topographic slope map showing fault traces in the eastern part of the Midorikawa fault zone. The extent of this map is indicated by the yellow box in Fig. 1b. Active fault traces are from Nakata and Imaizumi (2002). Active and inferred active fault traces are shown as solid and dashed black lines, respectively. Fault names are after ERC HERP (2013c). u, upthown side; d, downthrown side. Surface 1 is the depositional surface of the Aso-4 pyroclastic flow deposits. The background slope map was created from a 1-m grid digital elevation model provided by the Geospatial Information Authority of Japan. Black tick marks are coordinates in meters from Japan Plane Rectangular Coordinate System II.

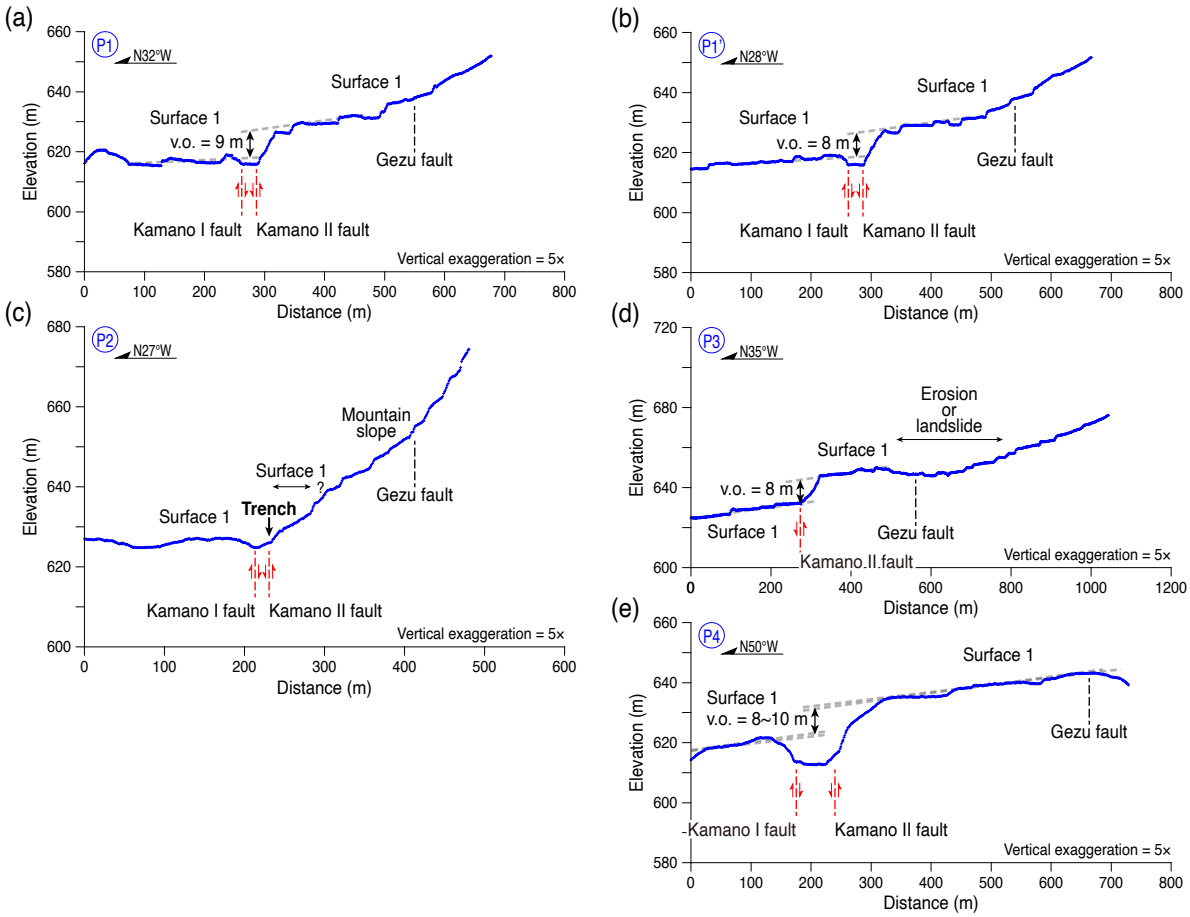

Fig. 3. Topographic profiles across fault traces P1–P4 (see locations in Fig. 2) in the eastern part of the Midorikawa fault zone. v.o., vertical offset of Surface 1 across the Kamano fault. The profiles are generated from 1-m grid digital elevation model provided by the Geospatial Information Authority of Japan. The Kamano I and Kamano II faults deform Surface I, forming a narrow graben-like depression. No topographic expression indicates recent faulting along the Gezu fault.

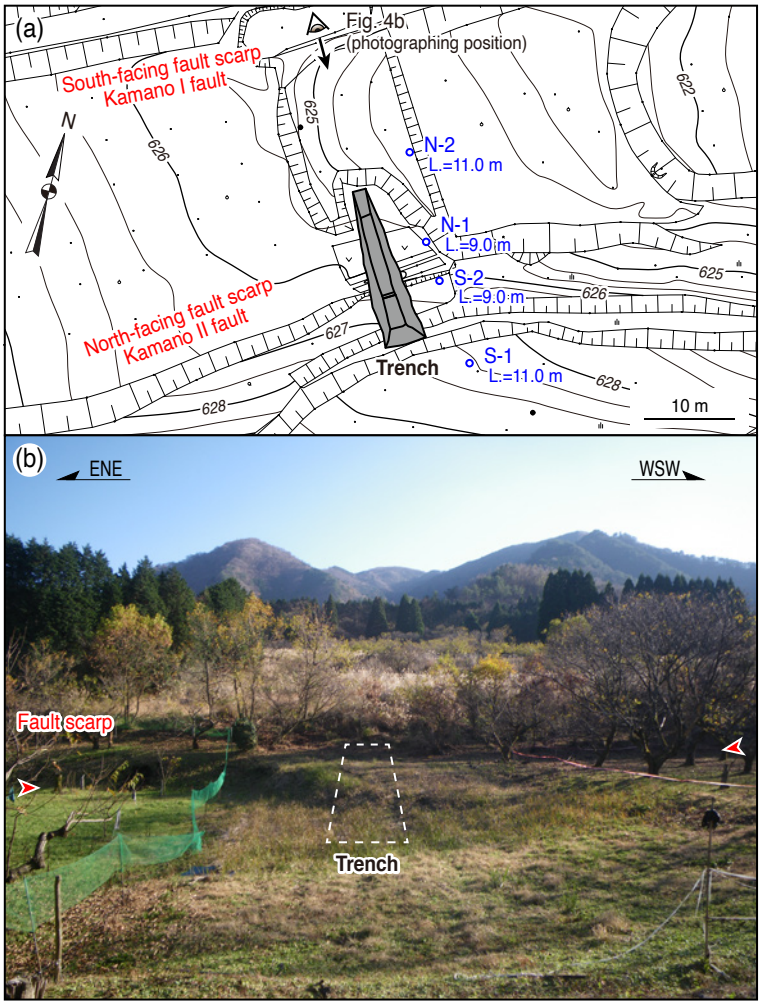

Fig. 4. (a) Survey map showing the layout of the trench and four coring points (blue circles) at the Kariya site. The location of this map is indicated on Fig. 2a. L., core length. (b) Photograph taken from the location shown in (a) looking south at the Kariya site. The trench crossed the *c*. 2 m high north-facing fault scarp of the Kamano II fault (red arrows).

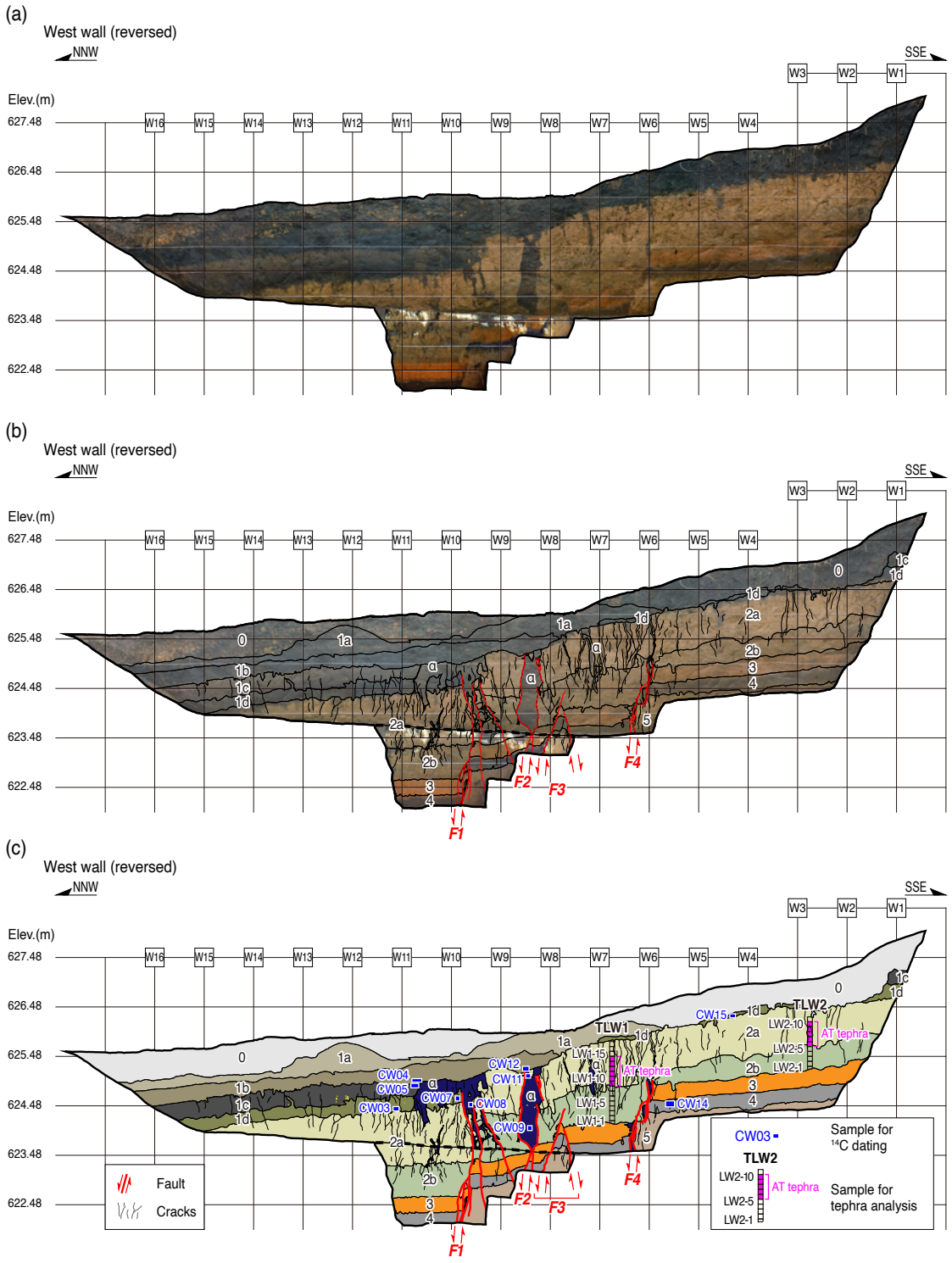

Fig. 5. (a) Uninterpreted photomosaic, (b) interpreted photomosaic, and (c) log of the west wall of the trench at the Kariya site. Images are flipped horizontally to facilitate comparison with the east wall. The area below the heavy dashed line between grids W7 and W12 was excavated after the initial excavation (see Fig. 7). Analyses of radiocarbon and tephra samples are listed in Tables 2 and 3, respectively.

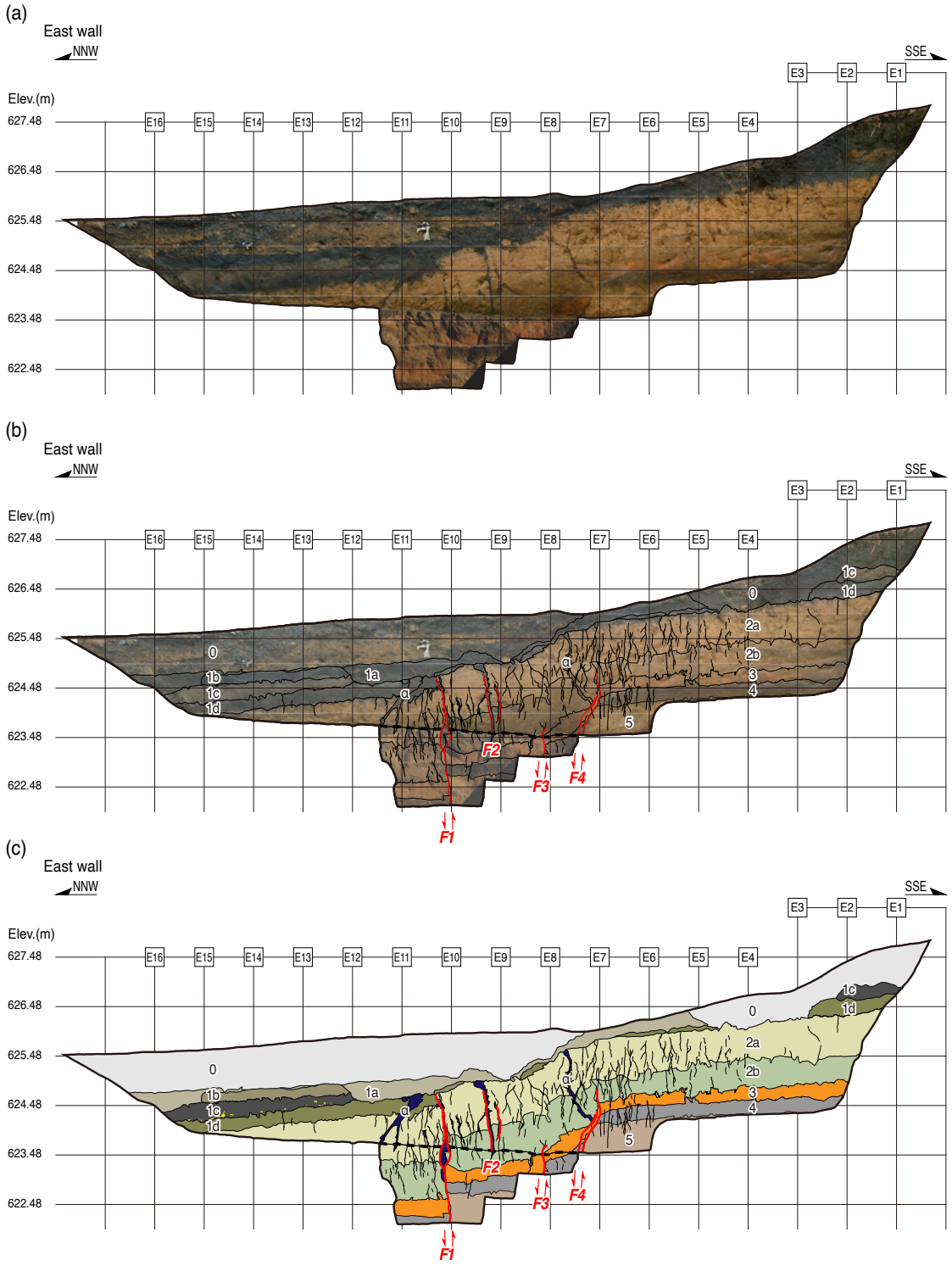

Fig. 6. (a) Uninterpreted photomosaic, (b) interpreted photomosaic, and (c) log of the east wall of the trench at the Kariya site. Details are as in Fig. 5.

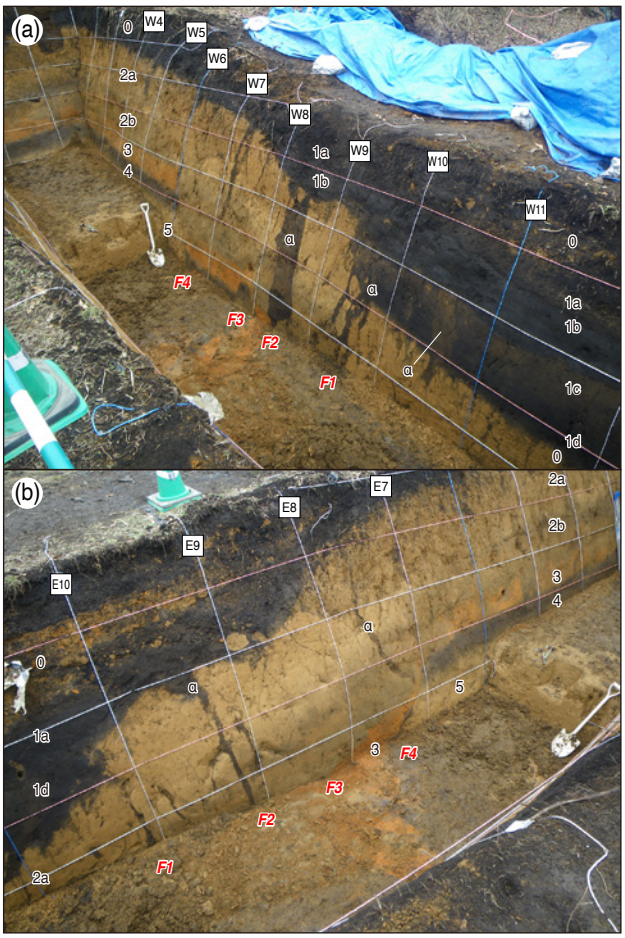

Fig. 7. Photographs of (a) the west wall and (b) the east wall of the trench at the Kariya site. Note that the photos were taken before the additional excavation on the downthrown side (see Figs. 5 and 6).

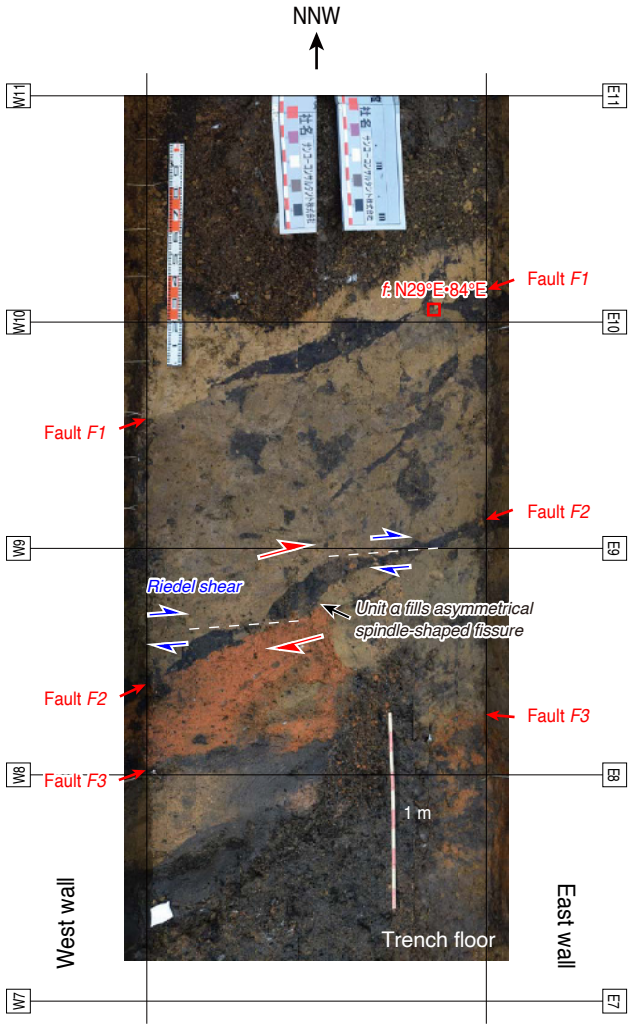

Fig. 8. Photograph of the trench floor before additional excavation, showing the geometry of faults and deformation between grids E7 (W7) and E11 (W11). Shear fabrics and the geometry of Unit α filling asymmetrical spindle-shaped fissures suggest the presence of a dextral slip component in addition to the north-side-down normal component. *f*, fault surface.

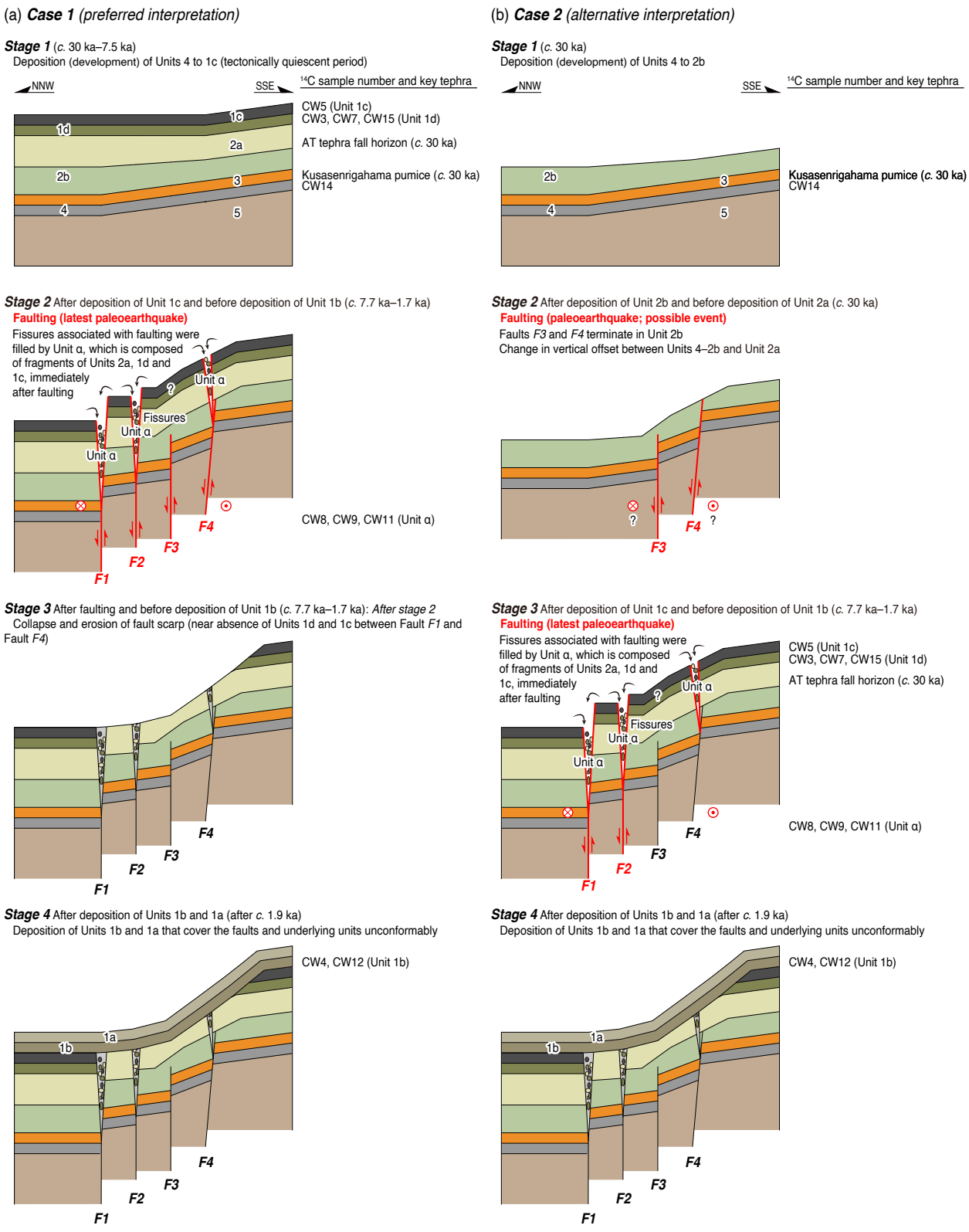

Fig. 9. Schematic cross sections showing the inferred evolution of the Kamano II fault as exposed at the Kariya site. (a) Our preferred interpretation with a single event occurring after the deposition of Unit 4 and (b) an alternative interpretation with two events occurring after the deposition of Unit 4. The alternative interpretation omits the "collapse and erosion" stage shown in the preferred interpretation. The ⊗ symbols indicate displacement away from the observer, and the ⊙ symbols indicate displacement toward the observer (i.e., dextral displacement).

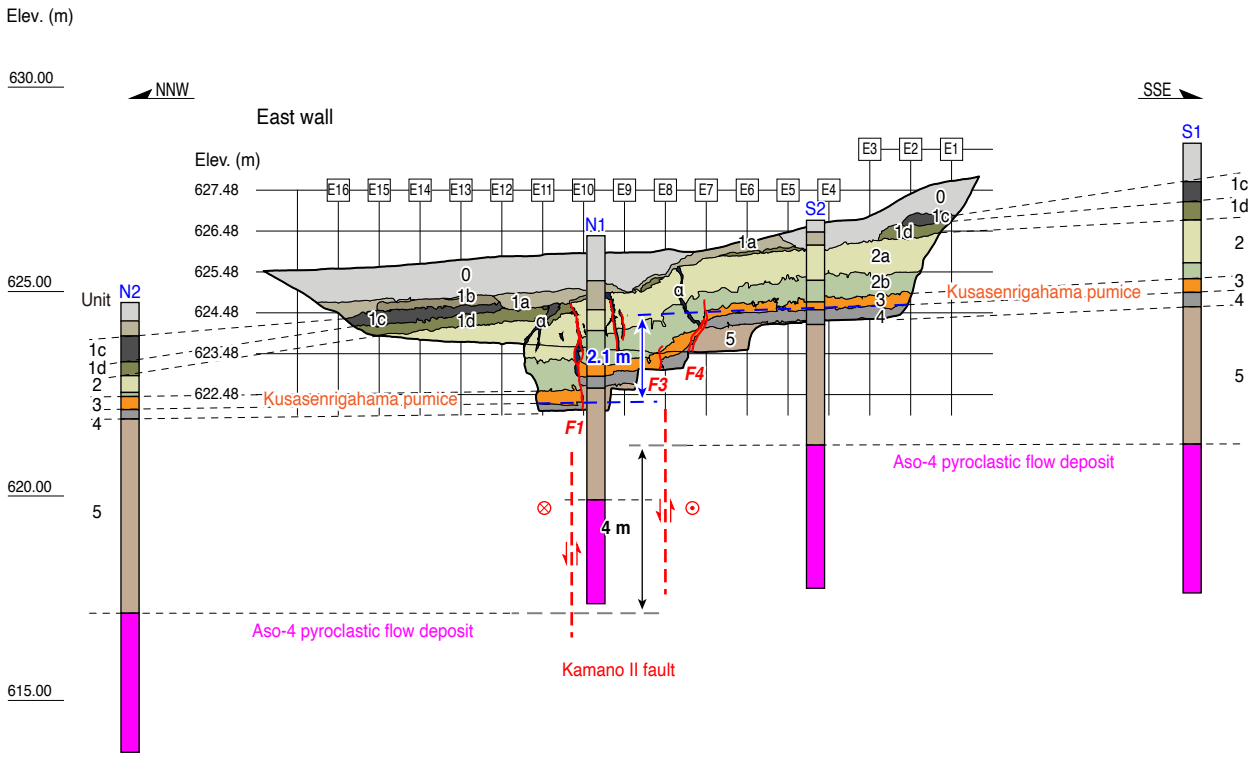

Fig. 10. Cross section across the Kamano II fault based on the trench logs and columnar sections of four boreholes at the Kariya site. The top of the Aso-4 pyroclastic flow deposits (~88–87 ka) is offset by 4 m across the fault whereas the trench documents a 2.1-m offset at shallower levels, possibly implying repeated faulting since the late Pleistocene. Borehole locations in Fig. 4a.